Sharp infrared eyes: the journey of QWIPs from concept to large inexpensive sensitive arrays in hand-held infrared cameras

S. GUNAPALA*, S. BANDARA, J. LIU, and M. SUNDARAM

Jet Propulsion Laboratory, California Institute of Technology
Pasadena, California 91109, USA

Arguably one of the simplest device realizations of the classic particle-in-a-box problem of basic quantum mechanics is the Quantum Well Infrared Photodetector (QWIP). Optimization of the detector design and material growth and processing has culminated in the realization of a portable infrared camera with a large (256×256 pixel) focal plane array of QWIPs which can see at 8.5 μm, holding forth great promise for a variety of applications in the 8–14 μm wavelength range. In this paper we discuss the physics and technology of the QWIP and report on the performance of the world's first hand-held infrared camera at these long wavelengths.

1. Introduction

Visible light spanning the wavelength range from blue (~ 0.4 μm) to red (~ 0.7 μm) is a tiny slice of the electromagnetic spectrum. While an enormous wealth of scientific information can be and is obtained through imaging and spectroscopy of objects in visible light, the invisible portion of the spectrum can be harvested to yield both more detailed and new information. Objects that are invisible to the human eye may be visible at other wavelengths. For instance, an object at room temperature (~ 300 K) and in complete darkness may be perfectly invisible to the human eye; but its temperature will make it glow in the infrared (IR) (at wavelengths longer than the 0.7 μm wavelength of red light), shining brightest at an IR wavelength of around 8.5 μm. A camera which can see 8.5 μm light and convert an 8.5 μm image to a visible black-and-white image on a standard TV monitor or camcorder viewfinder may make the invisible scene spring to life. Temperature and emissivity variations in the dark scene translate to contrast in the grey scale of the black-and-white image, rendering objects and

their motion visible. This is the basis of a night-vision camera. When fitted with filters to make it blind to visible light, such a camera, on viewing a human body in daylight, produces a contrasting black-and-white image that is a thermal map of the skin surface. Collapse the camera to a single detector, calibrate it to convert the IR radiation it sees to a temperature, and you have an infrared thermometer, the kind currently attached to most hospital beds.

While the invisible portion of the electromagnetic spectrum includes gamma rays, X-rays, and ultraviolet rays beyond the blue end of the visible spectrum, and infrared rays (spanning a wide wavelength swath from ~ 0.7 μm to ~ 1 mm) and microwaves beyond the red end, light detectors operating in the 8–14 μm wavelength range hold a special significance. Potential applications at these wavelengths range from the mundane to the sublime. As stated earlier, room temperature objects glow brightest in this wavelength range. Detectors with the sharpest eyes for light at these wavelengths are ideal for a variety of ground- and space-based applications such as night vision, early warning systems, navigation, flight control systems, weather monitoring, security and surveillance, etc. In addition, they can be used to monitor and mea-

*e-mail: Sarath.D.Gunapala@jpl.nasa.gov

sure pollution, relative humidity profiles, and the distribution of different gases (e.g., O_3, CO, N_2O, etc.) in the atmosphere. This is due to the fact that most of the absorption lines of gas molecules lie in this IR spectral region. The earth's atmosphere is opaque to most of the infrared; of its few transparent windows, the 8-12 μm is one of the clearest. Cameras operating in this wavelength range and used in ground-based telescopes will be able to see through the earth's atmosphere, image distant stars and galaxies (including those invisible to telescopes equipped with normal visible eyes), and help in the search for cold objects such as planets orbiting nearby stars. IR detectors operating in the 8-14 μm wavelength range thus find many applications in defence, commerce, and science.

At the heart of an IR camera (in its focal plane) is its eye; a 2-dimensional (2D) array of detector pixels, each pixel converting some of the IR photons hitting it to an electric signal. In front of the eye is a lens system to zoom and focus a scene onto the array. The eye can be made sharper by cooling, provided by a portable camera through a small Stirling cycle cooler (the eye is glued to the cold head and stares out through a sealed window in the surrounding vacuum jacket). The rest of the camera is its brains: the electronics that process the array output signals to produce a composite video signal that can be fed to a standard TV monitor. The image-processing electronics have advanced to the point where they can be packed into a few boards which fit inside a small box, while still allowing operator push-button control of all camera parameters in a simple and straightforward way. While impressive strides have been made in image processing chip design, the most dramatic advances in IR camera technology have been in the eye: in the ultimate analysis, a camera is only as good as its eye. The rest of the article will be devoted to a discussion of these advances. Henceforth, we also refer to light in terms of photons, each photon having an energy E = hν = hc/λ, where h is Planck's constant, and ν, c, and λ are the frequency, velocity, and wavelength of light, respectively.

The detector that constitutes each pixel in the 2D array can belong to one of two classes of detectors: photon detectors or thermal detectors. In a photon detector, some (ideally all) incident photons are absorbed, generating charge carriers (electrons and/or holes) which produce an electric signal which is a measure of the incident photon flux. In a thermal detector, some incident photons are absorbed, heating the detector material and changing some property; the change is measured and correlated to the incident photon flux. Photon detectors are fast, sensitive, and typically have narrow spectral responses, i.e., they can detect photons over limited wavelength ranges. Spectral response is a property of the detector material; detecting photons at a much different wavelength entails resorting to a different, more suitable detector material. Thermal detectors are slow, generally less sensitive, and have wide spectral responses (since they use the heating effect of photons, a process with usually simple wavelength dependence for most thermal detector materials). The more sensitive thermal detectors are also harder to fabricate into large arrays.

Given this scenario, the best IR cameras in the 3-20 μm wavelength range use photon detectors in their focal plane arrays (FPAs). The most common photon detectors are based on the principle of interband absorption in narrow bandgap semiconductors like InSb, $Hg_{1-x}Cd_xTe$, etc. IR radiation is absorbed by the photosensitive material when an incoming photon has sufficient energy E (= hν) to photoexcite an electron across the energy bandgap from the valence band to the conduction band. This process is equivalent to providing enough energy to free a valence electron (so called, because it is loosely bound to the atoms in the semiconductor crystal) and make it available for the conduction of electric current. Such a photoexcited electron is called a photoelectron. The hole that the photoelectron leaves behind is also now free to conduct electricity. Photons with energies less than the bandgap energy are not absorbed; they simply pass through the semiconductor. The bandgap energy therefore defines the low energy (or long wavelength cut-off) absorption edge of the detector. Applying a voltage bias across the detector creates an electric field that sweeps out both photocarriers producing a photocurrent in the external circuit. Such a detector need not be doped and is called an intrinsic detector. Large two-dimensional arrays of InSb (512×512 pixels) and $Hg_{1-x}Cd_xTe$ (128×128 pixels) detectors have already been demonstrated up to cut-off wavelengths of 5 μm and 11 μm respectively. The move to larger pixel arrays is driven by the need for greater scene resolution. Since the bandgap of InSb is fixed, InSb photodetectors cannot detect light at wavelengths longer than 5 μm. Longer wavelengths can be accessed by narrowing the bandgap of $Hg_{1-x}Cd_xTe$ by changing its alloy composition x. However, such narrow bandgap materials are more difficult to grow and process into devices, reducing the yield and increasing the cost of the arrays [2]. These difficulties motivate the exploration of artificial low effective bandgap structures built from
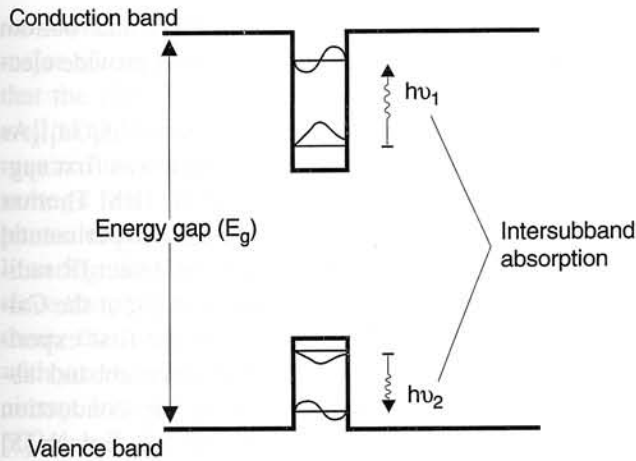
Conduction band

Fig. 1. Schematic band diagram of a quantum well. Intersubband absorption can take place between the energy levels of a quantum well associated with the conduction band or the valence band.

wide bandgap semiconductors such as GaAs (Fig. 1) which are far easier to grow and process into devices. A low effective bandgap can be created in a quantum well which resides entirely in either the conduction band or the valence band of a wide bandgap semiconductor like GaAs. Such a GaAs-based Quantum Well Infrared Photodetector (QWIP) then benefits from the highly mature GaAs growth and processing technologies, a benefit that becomes increasingly critical at the longer wavelengths where narrow bandgap materials become more tough to work with.

2. Multi quantum well IR detectors

The idea of using a quantum well to detect light can be understood by the basic principles of quantum mechanics. An electron in a square quantum well is the classic particle-in-a-box of basic quantum mechanics. The electron cannot have just any energy inside the well; rather, it is constrained to reside in certain discrete energy levels, i.e., its energy is quantized. These allowed energy levels, which depend on the electron mass and the size and shape of the quantum well, can be calculated by solving the time-independent Schrödinger wave equation. For a square quantum well (Fig. 1), the energy levels depend in a straightforward way on the well dimensions (width and potential depth). At low temperatures, an electron will reside in the lowest energy level (called the ground state) of the well. When a photon strikes the well, it can impart its energy to the ground state electron and excite it to the next allowed energy level (called the first excited state), a process called

intersubband absorption. In order for this to happen, the photon energy must equal the energy separation between the ground state and the first excited state. A photon with a different energy (i.e., light of a different wavelength) is not absorbed because there is no allowed energy state available for the photon to excite the ground state electron. The simplest QWIP design uses a simple square quantum well designed to hold just two states: a ground state deep inside the well, and the first excited state near the well top. A voltage bias can now be applied to sweep out the photoelectron; under constant illumination a steady-state photocurrent (a measure of the incident photon flux) thus flows through the detector. The spectral response of the QWIP is therefore quite narrow, its sharpness determined by the sharpness of the two energy states involved. Making a QWIP to detect light of a different wavelength is then simply accomplished by changing the width and potential depth of the well in such a way that the two energy states are separated by the corresponding photon energy.

Such a square quantum well can be created in the lattice-matched GaAs/Al_xGa_{1-x}As material system by sandwiching a layer of GaAs between two layers of Al_xGa_{1-x}As. The bandgap of Al_xGa_{1-x}As being larger than that of GaAs, results in a square quantum well for electrons in the conduction band: the GaAs layer is the well layer; the Al_xGa_{1-x}As layers on either side are the potential barriers. The depth of the potential well (= the height of the potential barrier) can be precisely controlled by controlling the Al mole fraction x in the Al_xGa_{1-x}As barrier layers. State-of-the-art crystal growth techniques like molecular beam epitaxy (MBE) permit the epitaxial growth of such layers, on a typically 3-inch diameter ~ 500-μm thick GaAs substrate, with ultra-high purity and with control of layer thickness down to a fraction of a molecular layer. This allows the width of the GaAs well layer (one of the design parameters) to be precisely controlled, and the interfaces between the well and barrier layers to be made truly sharp to produce a textbook square quantum well. A controlled number of ground state electrons are provided by doping the GaAs well with Si (an n-type dopant) during the MBE growth. It is worth noting that the above design also creates a square quantum well (with the same width but a smaller potential depth) for holes in the valence band. Ground state holes can be provided by doping the GaAs wells with Be (a p-type dopant) instead of Si, resulting in a QWIP in which holes, rather than electrons, are the photocarriers. The much heavier hole has poor trans-

port once it has been ejected out of the well by a photon, resulting in p-QWIPs being inferior in performance to n-QWIPs. We shall henceforth confine the discussion to electrons.

It is important to note that the quantum well exists only in one spatial dimension: the growth direction normal to the layers. While the electron energies are quantized in this direction, the electrons are essentially free to move about in the planes of the GaAs well layers. This has important consequences for the coupling of incident light, as will be explained later. The QWIP is thus a vertical device in that there is vertical transport of the electrons, perpendicular to the layers. The quantum wells in this material system can be designed to detect light at wavelengths longer than 5 µm (the wells cannot be made deep enough to detect shorter wavelength light). Several quantum wells (sandwiched between barriers) are usually grown stacked on top of each other to increase photon absorption. The upper limit on this number for a typical detector structure in this material system is around 50, about the number of wells and barriers that a photoelectron can traverse in an electric field without being captured by a well downstream from the well from which the electron originated. Fewer quantum wells implies less photon absorption; more implies fewer photoelectrons collected. Such a stack of quantum wells is called a multi quantum well (MQW) structure. The entire MQW stack is sandwiched between

heavily-doped top (called the emitter) and bottom (called the collector) GaAs layers which provide electrical contacts to the device.

The possibility of using such $GaAs/Al_xGa_{1-x}As$ MQW structures to detect IR radiation was first suggested by L. Esaki and H. Sakaki at the IBM Thomas J. Watson Research Labs [3]. The first experimental investigation of an MQW structure to detect IR radiation was carried out by J. Smith *et al.* [4] at the California Institute of Technology, and the first experimental observation of the strong intersubband absorption within quantum wells in the conduction band was performed by L. West and S.J. Eglash [5] at Stanford University. The first QWIP was demonstrated by B. Levine *et al.* at AT&T Bell Laboratories [6]. This QWIP was based on the intersubband transition between two bound quantum well states (i.e., both the ground state and the first excited state are inside the well). Absorption of a photon excites an electron from the ground state to the first excited state near the well top, where it can tunnel out to the continuum (continuous energy levels above the quantum well) in the presence of an external voltage bias, thereby producing a photocurrent.

The location of the first excited state relative to the top of the well can have a dramatic effect on device performance. By reducing the quantum well width it is possible to push this state up above the well top and into the continuum resulting in a strong bound-
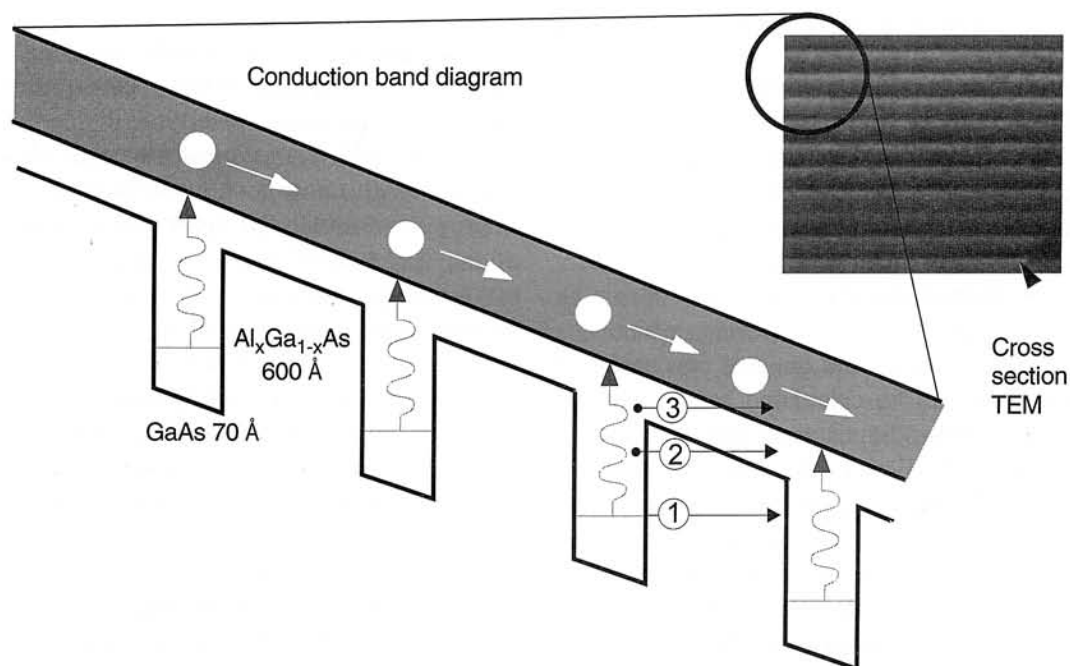

Fig. 2. A typical conduction-band diagram of very long wavelength bound-to-continuum quantum well infrared photodetector.

-to-continuum intersubband absorption (Fig. 2). The major advantage of the bound-to-continuum QWIP is that the photoelectron can escape from the quantum well to the continuum transport states without being required to tunnel through the barrier. As a result, the voltage bias required to efficiently collect the photoelectrons can be reduced dramatically, thereby lowering the dark current (see below). Furthermore, since the photoelectrons do not have to tunnel through them, the $Al_xGa_{1-x}As$ barriers can be made thicker without reducing the photoelectron collection efficiency. Increasing the barrier thickness from 200 Å to 500 Å reduces the ground state sequential tunnelling component of the dark current by an order of magnitude. Using all these improvements, B. Levine [6] at AT&T Bell Laboratories successfully demonstrated the first bound-to-continuum QWIP operating at 10 μm with a dramatic improvement in performance. Due to this high performance and the excellent uniformity of GaAs-based QWIPs, several groups have demonstrated large (two-dimensional arrays of 128×128, and 256×256 pixels) long wavelength IR (LWIR) imaging arrays [6-8] operating at temperatures up to 60 K.

3. Dark current

In addition to the photocurrent, all detectors including QWIPs produce a parasitic current called dark current which must be minimized to achieve high performance. The dark current is the current flowing through the detector when it is in the dark (i.e., with no photons impinging on it) and is ideally zero. In most applications the total current flowing through the detector is measured and there is no way to distinguish the dark current from the photocurrent. Though this dark current can be approximately subtracted in the image-processing electronics, a high dark current implies that the detector blinds itself even when it sees no photons; when it does see photons the image-processing electronics are swamped by the dark electrons with very little capacity left to process the photoelectrons. In QWIPs, the dark current originates from three different mechanisms, as shown in Fig. 2. The dark current arising from the first process is due to quantum mechanical tunnelling of ground state electrons from well to well through the $Al_xGa_{1-x}As$ barriers (sequential tunnelling). This process is independent of temperature. Sequential tunnelling domi-
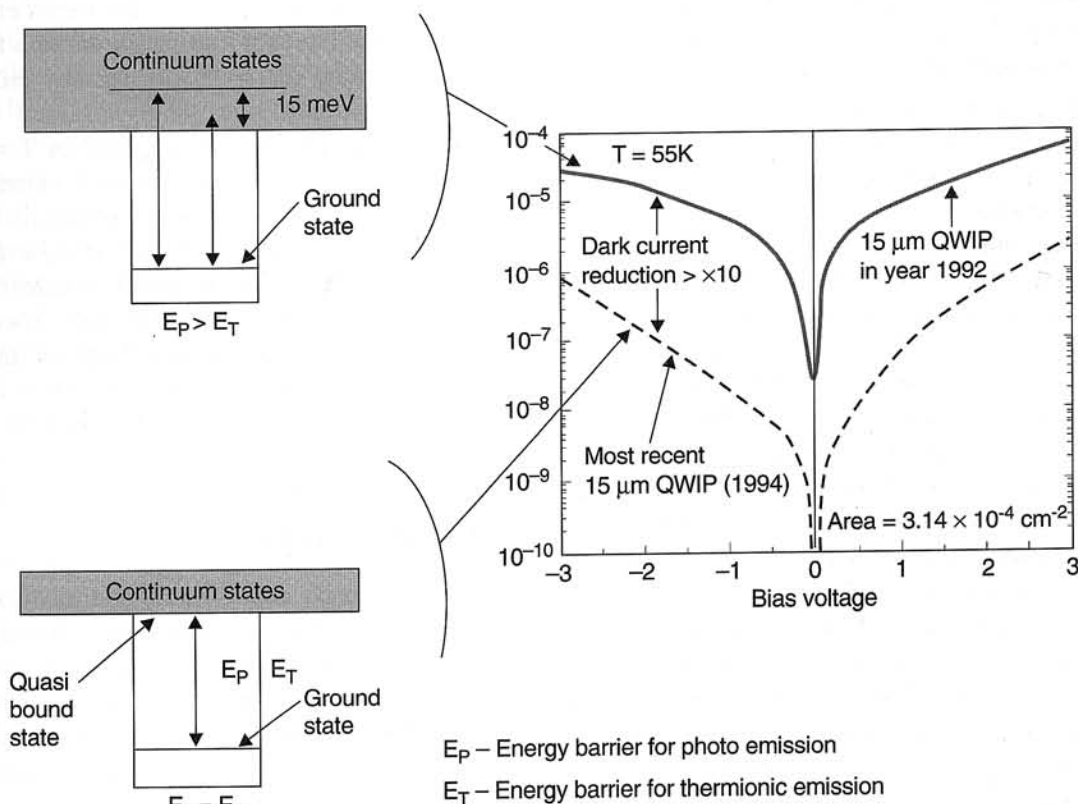

Fig. 3. Comparison of dark currents of bound-to-continuum and bound-to-quasibound LWIR QWIPs as a function of bias voltage at temperature T = 70 K. Data was taken with a 200 μm diam test structure and normalised to 28×28 μm² pixel.

nates the dark current at very low temperatures (< 30 K). The second mechanism is thermally assisted tunnelling which involves thermal excitation of a ground state electron followed by its tunnelling through the tip of the barrier into the continuum energy levels. This process governs the dark current at medium temperatures. The third mechanism is classical thermionic emission (the emission of electrons over a finite potential barrier due to their finite temperature) and dominates the dark current at higher temperatures (> 45 K). Reducing the dark current due to this mechanism is critical to the commercial success of the QWIP since it enables the highly desirable higher temperature camera operation.

The thermal generation rate of electrons is determined partly by their lifetime, which in turn is determined by the thickness of the $Al_xGa_{1-x}As$ barriers, as described by E. Rosencher *et al.* at the Thomson-CFS Research Laboratory, France [9]. The dark current can be reduced by increasing the barrier thickness to the point beyond which any further increase would reduce the photocurrent (by a reduction in the efficiency of collection of photoelectrons). The thermal generation rate also depends on the number of electrons (i.e., doping density) in the well. Increasing this number increases the photocurrent; unfortunately, it also increases the dark current. This dependence was analysed by S. Gunapala *et al.* at AT&T Bell Laboratories [10]. In particular, they found that the dark current could be reduced by many orders of magnitude by lowering the well doping density, without significantly reducing the performance of the detectors. For a QWIP designed to detect light at a desired wavelength, there is thus an optimum barrier thickness and well doping density which will minimise the dark current without sacrificing too much in terms of lost photocurrent.

Another trick to reduce the dark current due to thermionic emission and optimise the performance of LWIR QWIPs has been devised by S. Gunapala and K. Bandara at the Jet Propulsion Laboratory [11]. This QWIP uses bound-to-quasibound intersubband absorption (occurring when the first excited state is in resonance with the top of the well). This transition maximises the intersubband absorption while maintaining excellent electron transport. The major advantage of this design lies in the fact that it increases the energy barrier to thermionic emission compared to the case of the bound-to-continuum QWIP (Fig. 3). The energy barrier to thermionic emission is the potential height from the ground state to the well top. In the case of the bound-to-continuum QWIP, the energy

barrier to thermionic emission is about 10–15 meV less than the barrier to photon absorption (since the first excited state is about 6 meV above the well top). In the case of the bound-to-quasibound QWIP, the two barriers are equal. If the two QWIPs are designed to detect the same photon energy (= the barrier to photon absorption) the bound-to-quasibound design thus has a 10–15 meV higher energy barrier to thermionic emission than the bound-to-continuum QWIP, an increase which will drop its dark current by a factor of 10 (i.e., $I_d \propto \exp(-\Delta E/kT) \approx e^{-1}$ for T = 70 K). One could push the first excited state deeper into the well to increase the energy barrier to thermionic emission even further, but this would drop the photocurrent to unacceptably low levels. The bound-to-quasibound QWIP preserves the photocurrent while reducing the dark current.

A bound-to-quasibound QWIP operating at a peak wavelength λ_p = 8.5 μm typically consists of a 45 Å wide GaAs quantum well sandwiched between 500 Å thick $Al_xGa_{1-x}As$ barriers with x ≈ 0.3. The device structure is grown by MBE and consists of 50 periods of quantum wells and barriers, sandwiched between 0.5 μm top and 1 μm bottom Si-doped (N_D = $1{\times}10^{18}$ cm^{-3}) contact layers. The quantum well doping density is substantially reduced to N_D = $5{\times}10^{17}$ cm^{-3}, in order to lower the Fermi energy (E_F) of the carriers (so as not to be too large a fraction of the cutoff energy E_C = hc/λ_c), thereby reducing the thermal generation rate. The measured dark current-voltage curve of such a QWIP at T = 55 K is shown in Fig. 3 along with the dark current-voltage curve of a 15 μm peak bound-to-continuum QWIP for comparison. As stated above, the virtual excited level of this bound-to-continuum QWIP is calculated to be ~ 15 meV above the top of the well. Theoretically, this should reduce the dark current of the bound-to-quasibound QWIP by a factor of ~ 10, which agrees well with the reduction factor of 12 measured at voltage bias V_B = –2 V.

4. Light coupling

In order to be absorbed by the electrons in the quantum wells, the incoming light should have an electric field component in the quantum well direction, i.e., in the growth direction, normal to the layers. Only in this situation is the electric field of the light coupled to the quantised electron momentum, enabling a photon to excite an electron and get absorbed in the process. Light being a transverse wave (whose electric field is perpendicular to the direction of

travel), this selection rule means that light striking the layers normally (the most direct way to illuminate an imaging array of detectors) is not absorbed. If the light is sent through the thin (~ 500 µm) edge of the detector it can be absorbed since it now has a component of its electric field in the correct direction. The edge is sometimes given a 45° wedge and the incident light focused normally on the polished edge facet [6]. Both schemes result in incident light being piped laterally through the detector. This clearly limits the configuration of detectors to linear arrays and single elements. For imaging, it is necessary to be able to couple light uniformly to two-dimensional arrays of detectors. An elegant way to couple normally incident light to an imaging array of QWIPs is to use a grating to bend some of the light inside the detectors.

This is accomplished by putting a special reflector on the detector top and illuminating the detector from the back. If the reflector is a smooth mirror, it is useless: the normally incident light passes through the detector, strikes the mirror, and is reflected straight back out of the back side with none of the light being absorbed by the confined electrons. To be useful, the mirror has to be rough (on the scale of the wavelength of the light in the detector's GaAs material). This roughness may be either periodic or random (Fig. 4). A rough mirror scatters or sprays the incident light back in a cone (i.e., the roughness ensures that the angle of reflection no longer equals the angle of incidence). The details of the cone depend on the details of the roughness. This cone now strikes the bottom side. Those rays that are within a critical angle of the normal (17° for the GaAs-air interface) refract or escape back into the air. The rest suffer total internal reflection with the back surface acting as a smooth mirror. The internally reflected rays are once again reflected off the top rough mirror. What happens next depends on whether the roughness of the top mirror is periodic or random. If it is periodic, the top mirror will scatter or bend these rays so that they are all normal to the quantum well layers again. These rays pass through the detector and out of the backside. A randomly roughened mirror, on the other hand, will randomly reflect or scatter all the rays internally reflected on to it from the bottom side each time, thereby allowing the incident light to bounce back and forth between the detector top and back surfaces several times. Only light within a 17° (from normal) cone escapes out of the backside. Clever design can reduce the amount of light in the escape cone but cannot eliminate it altogether. For instance, if the random reflector is designed with two levels of rough surfaces
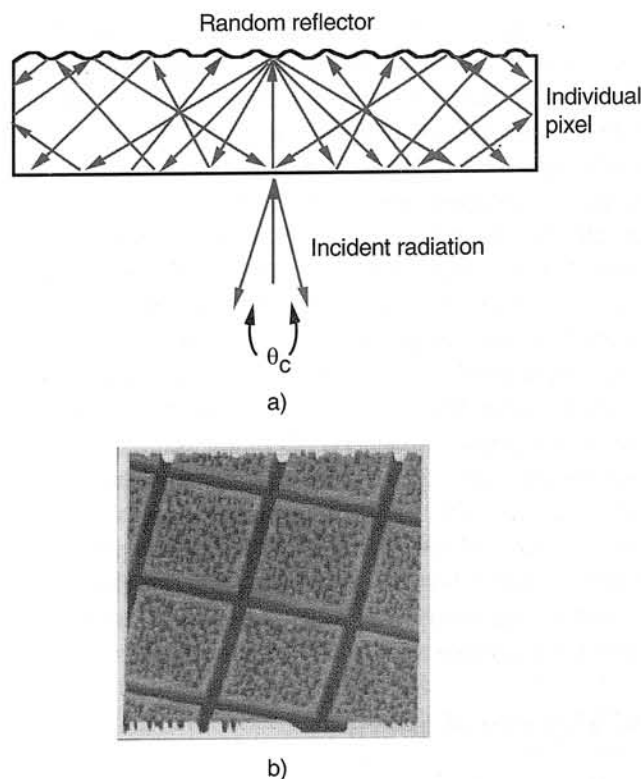

Fig. 4. Schematic side view of a thin QWIP pixel with a random reflector: (a) ideally all the radiation is trapped: except for a small fraction which escape through the escape cone (defined by critical angle θ_c), (b) random reflectors on pixels in a focal plane array.

having the same areas but located a quarter wavelength ($\lambda_{GaAs}/4$) apart, the normally reflected light intensities from the top and bottom surfaces of the reflector are equal and 180° out of phase. This maximizes the destructive interference at normal reflection and lowers light leakage through the escape cone.

On each pass through the detector following the first reflection off the top rough mirror, some of the light is absorbed by the confined electrons since most of the light rays now have an electric field component in the correct direction (normal to the quantum well layers). A periodically roughened mirror thus yields two useful passes; a randomly roughened mirror offers several. One measure of the resulting efficiency of the detector in absorbing photons is its responsivity (the photocurrent for a given incident photon flux). Under identical conditions, a top reflector with one-dimensional periodic roughness will give a QWIP about the same responsivity that it would have if illuminated through a 45° edge facet; both the reflector with two-dimensional periodic roughness as well as the random reflector will approximately double this responsivity. Squeezing

the maximum light trapping ability from the reflector requires increasing the detector aspect ratio, i.e., the ratio of detector diameter to height, a design feature accomplished by thinning the ~ 500 μm thick GaAs substrate on top of which the detector material is grown, to about zero. The resulting optical cavity is calculated and measured to improve the responsivity of a QWIP with a random reflector significantly over the 45° case [12]. Thinning enhances the responsivities of the QWIPs with 1D and 2D periodically rough reflectors to be respectively about 2 and 4 times better than the 45° case. The random reflector is fabricated on the QWIPs using standard photolithography and CCl_2F_2 selective dry etching. The advantage of the photolithographic process over a completely random process is the ability to accurately control feature size and preserve the pixel-to-pixel uniformity necessary for very sensitive imaging focal plane arrays.

Fig. 5. Typical photoresponse curves of bound-to- continuum and bound-to-quasibound QWIPs at temperature T = 77 K.

5. Figures of merit

Responsivity and detectivity are two figures of merit commonly used to compare the performance of detectors. Responsivity is the ratio of the signal current to the incident radiation power on the QWIP. The higher the responsivity, the more sensitive the detector. Figure 5 shows typical photoresponse curves of long wavelength bound-to-continuum and bound-to--quasibound test QWIPs at temperature T = 77 K. The absorption and photoresponse curves of the bound-to--continuum QWIPs are much broader than those of the bound-to-quasibound QWIPs. This is because the first excited state, being in the continuum, is broader in the former than in the latter. The responsivity of the bound-to-quasibound QWIP peaks at 8.5 μm with a peak (R_p) value of 300 mA/W at bias $V_B = -3$ V. The spectral width and cutoff wavelength are $\Delta\lambda/\lambda = 10\%$ and $\lambda_c = 8.9$ μm, respectively. The peak quantum efficiency (a measure of the number of photoelectrons generated by each photon striking the QWIP) of the bound-to-quasibound QWIP is 6.9% at bias $V_B = -1$ V. Detectivity (D^*) is the signal-to-noise ratio normalised to unit area and unit bandwidth. The primary noise source in QWIPs is the shot noise produced by the dark current. Therefore, unlike the narrow bandgap detectors in which the noise is dominated by temperature-independent processes at low temperatures, the QWIP performance can be further improved by cooling to cryogenic temperatures to further reduce the dark current. Rapid progress has been made in the performance (detectivity) of very
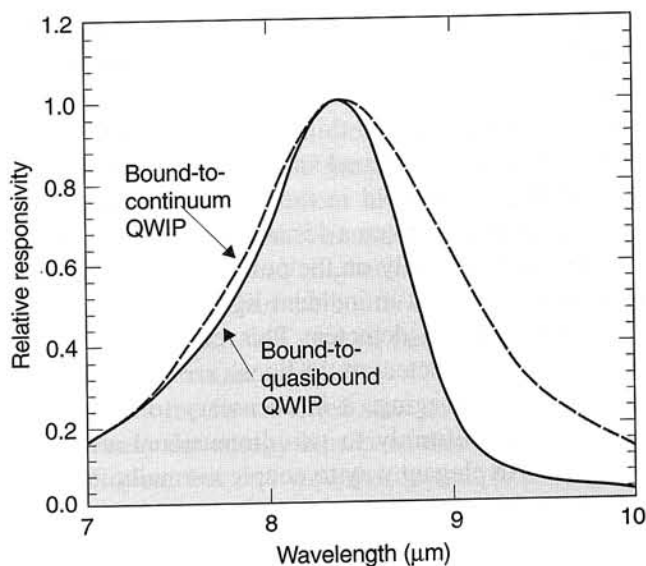
long wavelength QWIPs, starting with bound-to--bound QWIPs which had relatively poor sensitivity, and culminating in high performance bound-to-quasibound QWIPs with random reflectors. The achieved detectivities are more than sufficient to demonstrate large two-dimensional imaging arrays (640×512 pixels or larger) at long wavelength, which is presently not possible with intrinsic narrow bandgap detectors.

Due to pixel-to-pixel nonuniformities, the detectivity of a single pixel is not sufficient to describe the performance of a large imaging array. The noise induced by this nonuniformity has to be taken into account for a complete evaluation. This point has been discussed in detail by F. Shepherd [14] at the U.S. Air Force Rome Laboratories for the case of PtSi infrared focal plane arrays which have low response, but very high uniformity. The general figure of merit to describe the performance of a large imaging array is the noise equivalent temperature difference (NEΔT), which includes the spatial noise originating from pixel-to-pixel nonuniformities. NEΔT is the minimum temperature difference across the target that would produce a signal-to-noise ratio of unity, and is a measure of the minimum resolvable temperature difference in a scene.

6. Imaging arrays

The imaging arrays were fabricated as follows. After the random reflector array was defined by lithography and dry etching, the photoconductive QWIPs of
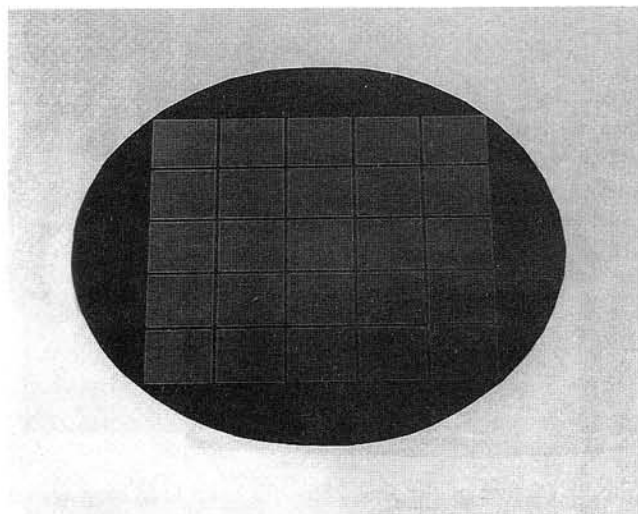
Fig. 6. Twenty-five 256×256 QWIP focal plane arrays on a 3 in. GaAs wafer.

the 256×256 pixel FPAs were fabricated by wet chemical etching of trenches (to isolate each QWIP pixel from its neighbours) through the photosensitive

GaAs/Al$_x$Ga$_{1-x}$As multi-quantum well layers into the 0.5 μm thick doped GaAs bottom contact layer. The pitch of the FPA is 38 μm; the actual pixel size is 28×28 μm. The random reflectors on the tops of the detectors were then covered with Au/Ge and Au for ohmic contact and reflection. Figure 6 shows a picture of twenty-five 256×256 pixel QWIP FPAs on a 3-inch GaAs wafer, produced by the Jet Propulsion Laboratory. Indium bumps were then evaporated on the tops of the detectors for Si readout circuit (ROC) hybridisation. A single QWIP FPA was chosen and hybridized or mated (via an indium bump-bonding process as shown in Fig. 7) to a matching 256×256 pixel CMOS multiplexer (Amber AE-166), and biased at V_B = −1 V.

At temperatures below 72 K, the signal-to-noise ratio of the system is limited by array non-uniformity, multiplexer readout noise, and photo current (photon flux) noise. At temperatures above 72 K, temporal noise due to the QWIP's higher dark current becomes the limitation. The FPA was back-illuminated through the flat thinned substrate membrane (thickness
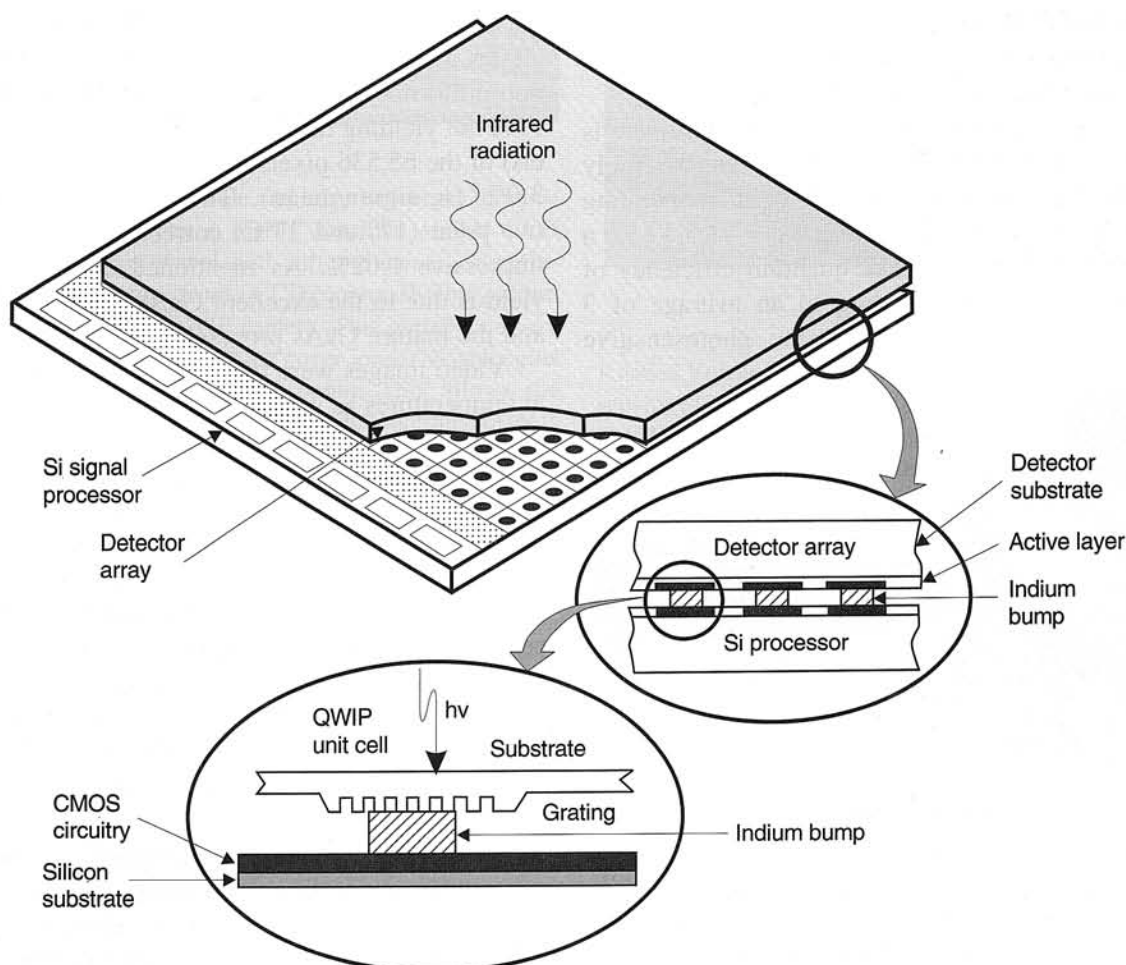

Fig. 7. Cross-section of 256×256 QWIP FPA and silicon CMOS multiplexer hybrid.

$\approx$ 1300 Å). The measured mean NEΔT of the FPA with no lens was 26 mK at an operating temperature of T = 70 K and bias $V_B = -1$ V, for a 300 K background. This initial array gave excellent images with 99.98% of the pixels working (number of dead pixels $\approx$ 10), demonstrating the high yield of GaAs technology.

7. Hand-held camera

A 256×256 QWIP FPA hybrid was mounted on to a 450 mW integral Sterling closed-cycle cooler assembly (shown in Fig. 8) and installed into an Amber RADIANCE 1™ camera-body, to demonstrate a hand-held LWIR camera (shown in Fig. 9). The camera is equipped with a 32-bit floating-point digital signal processor combined with multi-tasking software, providing the speed and power to execute complex image-processing and analysis functions inside the camera body itself. The other element of the camera is a 100 mm focal length germanium lens, with a 5.5-degree field of view. It is designed to be transparent in the 8-12 µm wavelength range, to be compatible with the QWIP's 8.5 µm operation. The digital acquisition resolution of the camera is 12-bits. Its nominal power consumption is less than 50 Watts.

The measured mean NEΔT of the QWIP camera is 40 mK (the higher NEΔT is due to the lens assembly cutting the light transmission by 35%) at an operating temperature of T = 70 K and bias $V_B = -1.5$ V, for a 300 K background. The peak quantum efficiency of the FPA is 3%, corresponding to an average of 3 passes of IR radiation through the photosensitive
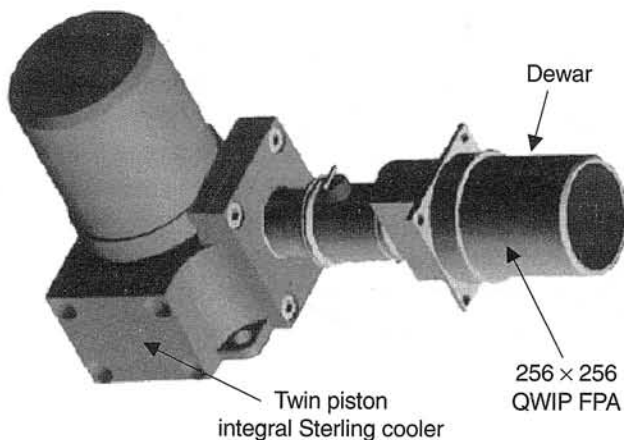

Fig. 9. Picture of the first 256×256 hand-held long wavelength QWIP camera (QWIP RADIANCE).

multi-quantum well region. The low quantum efficiency can be partly attributed to the fact that the substrate reflects 30% of the light striking it; and the fact that the array has a 65% fill factor, i.e., the detectors cover only 65% of the array surface, with the remaining 35% being the dead space between detectors. The uncorrected photocurrent non-uniformity (which includes a 1% non-uniformity of the ROC and a 1.4% non-uniformity due to the cold-stop in front of the FPA not yielding the same field of view to all the pixels) of the 65,536 pixels of the 256×256 FPA is about 3.0% (= sigma/mean). The non-uniformity after two-point (17° and 27°C) correction improves to an impressive 0.02%. As mentioned earlier, this high yield is due to the excellent GaAs growth uniformity and the mature GaAs processing technology.

Video images were taken at a frame rate of 60 Hz at temperatures as high as T = 70 K, using a ROC capacitor having a charge capacity of 9×10^6 electrons (the maximum number of photoelectrons and dark electrons that can be counted in the time taken to read each detector pixel). This infrared camera helped a Los Angeles TV news crew get a unique perspective on fires that raced through the Southern California seaside community of Malibu in October, 1996. The camera hopped a flight on the station's news helicopter. This portable camera features infrared detectors which cover longer wavelengths than previous portable cameras could. This allows the camera to see through smoke and pinpoint lingering hotspots which are not normally visible. This enabled the TV station to transmit live images of hotspots in areas which appeared innocuous to the naked eye. These hotspots are a source of concern and difficulty for firefighters, because they can flare up even after the fire appears to

Fig. 8. Picture of the QWIP camera's sensor engine, which combines advanced 256×256 QWIP FPA and twin piston integral Sterling cooler. This cooler is capable of providing cooling capacities exceeding 450 mW at 70 K in a standard room temperature environment of 23°C.
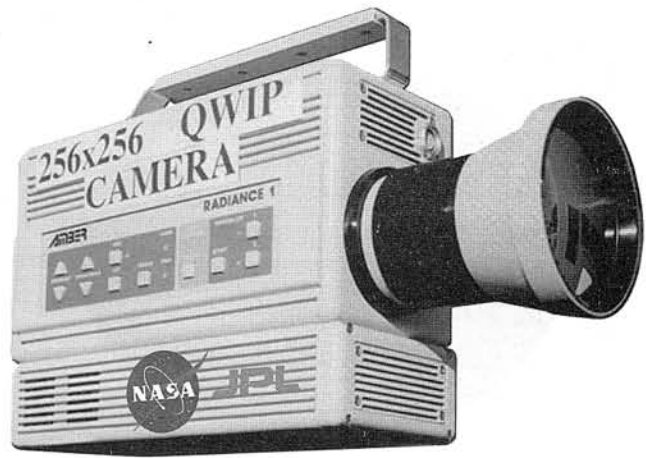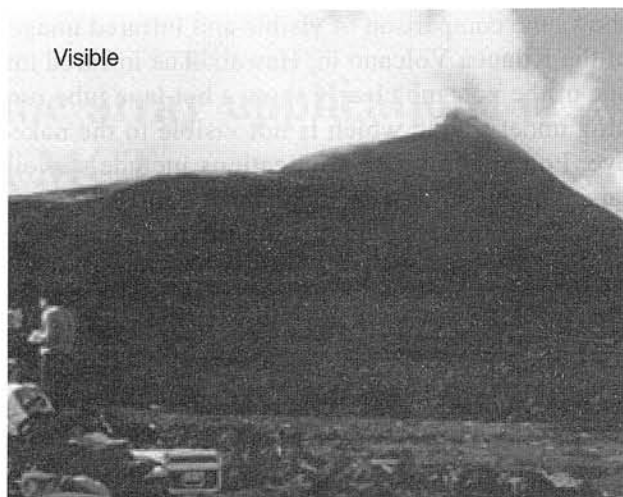
a)

b)

Fig. 10. Comparison of visible and infrared images of a just burned area as seen by a highly sensitive visible CCD camera and the long wavelength infrared camera in night-time. (a) Visible image from a CCD camera. (b) Image from the 256×256 portable QWIP camera. This portable camera features infrared detectors which cover longer wavelengths than previous portable cameras could. This allows the camera to see through smoke and pinpoint lingering hotspots which are not normally visible. This enables fire-fighters to locate the hotspots in areas which appeared innocuous to the naked eye. These hotspots are a source of concern and difficulty for firefighters, because they can flare up even after the fire appears to have subsided. It works effectively in both daylight and night-time conditions.

a)

b)

Fig. 11. Comparison of visible and infrared images of the Kilauea Volcano in Hawaii: (a) visible image from a highly sensitive CCD camera, (b) image from the 256×256 portable QWIP camera. The wide dynamic range enabled us to image volcanic features at temperatures much higher (300–1000°C) than can be imaged with conventional thermal imaging systems in the 3–5 μm range or in visible. The infrared image of the volcano clearly show a hot lava tube running underground which is not visible to the naked eye. This demonstrates the advantages of long wavelength infrared in geothermal mapping.

have subsided. Figure 10 shows the comparison of visible and infrared images of a just burned area as seen by the news crew in night-time. It works effectively in both daylight and night-time conditions. The event marked the QWIP camera's debut as a fire-observing device.

In addition, the camera has been used to observe volcanoes, mineral formations, weather and atmo-spheric conditions. This QWIP camera was taken to the Kilauea Volcano in Hawaii. The objectives of this trip were to map geothermal features. The wide dynamic range enabled us to image volcanic features at temperatures much higher (300–1000°C) than can be imaged with conventional thermal imaging systems in the 3–5 μm range or in visible. Figure 11

shows the comparison of visible and infrared images of the Kilauea Volcano in, Hawaii. The infrared image of the volcano clearly show a hot lava tube running underground which is not visible to the naked eye. Potential civilian applications include surveillance, night vision and sophisticated medical imaging. These images demonstrate the high sensitivity of the 256×256 QWIP staring array camera.

8. Conclusions

Exceptionally rapid progress has been made in the development of long wavelength QWIPs [16], since they were first experimentally demonstrated several years ago. It is now possible for QWIPs to achieve excellent performance (e.g., detectivities as high as $D^* \sim 1\times10^{11}$ cm$\sqrt{\text{Hz}}$/W at 70 K for a 9 μm QWIP) and be fabricated into large inexpensive low-noise imaging arrays. A 70 K operating temperature can be easily achieved by single-stage Stirling cycle coolers, which allows us to demonstrate the first hand- -held 256×256 FPA LWIR camera based on QWIPs. Weighing about ten pounds, the QWIP RADIANCE 1 camera is entirely self-contained, with no extra boxes for control, cooling, or image processing. Its sharp, inexpensive, large, uniform, infrared eye (which can be tailored to see a particular IR wavelength) makes the QWIP hand-held camera the best and the most cost-effective new tool for imaging and spectroscopy in the interesting 8-14 μm wavelength range.

Acknowledgements

References

1. M.T. Chahine, *Proc. Innovative Long Wavelength Infrared Detector Workshop*, Pasadena, California, 1990.
2. B.F. Levine, *Appl. Phys. Lett.* **56**, 2354 (1990).
3. L. Esaki and H. Sakaki, *IBM Tech. Disc. Bull.* **20**, 2456 (1977).
4. J.S. Smith, L.C. Chiu, S. Margalit, A. Yariv, and A.Y. Cho, *J. Vac. Sci. Technol.* **B1**, 376 (1983).
5. L.C. West and S.J. Eglash, *Appl. Phys. Lett.* **46**, 1156 (1985).
6. B.F. Levine, *J. Appl. Phys.* **74**, R1 (1993).
7. L.J. Kozlowski, G.M. Williams, G.J. Sullivan, C.W. Farley, R.J. Andersson, J.Chen, D.T. Cheung, W.E. Tennant, and R.E. DeWames, *IEEE Trans. Electron. Devices* **ED-38**, 1124 (1991).
8. W.A. Beck, T.S. Faska, J.W. Little, J. Albritton, and M. Sensiper, *2nd International Symposium on 2-20 μm Wavelength Infrared Detectors and Arrays: Physics and Applications*, Miami Beach, Florida, 1994.
9. E. Rosencher, F. Luc, P. Bois, J. Nagle, and Y. Cordier, *Appl. Phys. Lett.* **63**, 3312 (1993).
10. S.D. Gunapala, B.F. Levine, L. Pfeiffer, and K. West, *J. Appl. Phys.* **69**, 6517 (1991).
11. S.D. Gunapala and K.M.S.V. Bandara, *Physics of Thin Films*, Academic Press, Vol. 21, 113 (1995).
12. G. Sarusi, S.D. Gunapala, J.S. Park, and B.F. Levine, *J. Appl. Phys.* **76**, 6001 (1994).
13. G. Sarusi, B.F. Levine, S.J. Pearton, K.M.S.V. Bandara, and R.E. Leibenguth, *Appl. Phys. Lett.* **64**, 960 (1994).
14. F.D. Shepherd, in *Infrared Detectors and Arrays*, SPIE, Orlando, Florida, Vol. 930, p. 2 (1988).
15. S.D. Gunapala, J.K. Liu, J.S. Park, M. Sundaram, C.A. Shott, T. Hoelter, True-Lon Lin, S.T. Massie, P.D. Maker, R.E. Muller, and G. Sarusi, *IEEE Trans. Electron Devices* **44**, 51 (1997).
16. S.D. Gunapala, S.V. Bandara, J.K. Liu, W. Hong, M. Sundaram, P.D. Maker, R.E. Muller, C.A. Shott, and R. Carralejo, *IEEE Trans. Electron Devices* **45**, 1890 (1998).